



Research papers

Roles of the stolon and erect grass species in surface–subsurface flow generation and red soil loss



Zhimin Yang^{a,b}, Chunhui Li^b, Yaojun Liu^{a,c,*}, Jian Duan^c, Lichao Zhang^d, Zhongwu Li^a, Xiangyu Zhou^a, Qi Li^a, Yichun Ma^a, Liang Tian^a

^a School of Geographic Sciences, Hunan Normal University, Changsha, 410081, China

^b School of Environment, Beijing Normal University, Beijing 100875, China

^c Jiangxi Provincial Key Laboratory of Soil Erosion and Prevention, Nanchang 330029, China

^d Nanchang Institute of Technology, Nanchang 330099, China

ARTICLE INFO

Keywords:

Surface–subsurface flow
Sediment
Hydraulic and hydrodynamic characteristics
Grass species
Rainfall simulation

ABSTRACT

Grass planting is an important and typical measure for soil and water conservation, while the roles of stolon and erect grass species in affecting surface–subsurface flow and soil erosion processes are little understood. Experimental plots ($2\text{ m} \times 0.5\text{ m} \times 0.5\text{ m}$) using red soil with two rainfall intensities (60 and 120 mm h^{-1}) and grass coverage (30% and 70%) were conducted in laboratory rainfall simulation experiments. Two common and endemic stolon (*Eremochloa ophiurooides*) and erect (*Lolium perenne*) grass species were selected due to their fast growth, power adaptability, and wide application in reducing runoff and soil loss; and the bare soil plot was set up as the control. The results showed that bare plot had the highest mean surface flow coefficient (73.5%), and then were *L. perenne* (57.1%) and *E. ophiurooides* (44.9%). The mean subsurface flow coefficients were found in order of *E. ophiurooides* (25.7%), *L. perenne* (13.0%) and bare plot (7.2%). The role of stolon grass rather than erect grass in reducing surface flow but improving subsurface flow led to lower surface flow hydraulic characteristics such as flow velocity, Reynolds number, Darcy–Weisbach coefficient and Manning friction coefficient, and hydrodynamic characteristics like flow shear stress and stream power. Furthermore, the stolon grass generated the lowest soil loss rate ($0.8\text{ g m}^{-2}\text{ min}^{-1}$), while the values on erect grass and bare plot were 2.5 and $10.7\text{ g m}^{-2}\text{ min}^{-1}$, respectively. The indicator of eroded sediment median size also proved the higher efficiency of stolon grass in soil loss control, with values of 31.8 , 58.6 and $69.6\text{ }\mu\text{m}$ on stolon grass, erect grass and bare plots, respectively. The lower soil loss on stolon grass cover plot was attributed to the lower surface flow and hydraulic–hydrodynamic characteristics. The stolon grass was more sensitive to the coverage and rainfall intensity, which was explained by the higher flow and sediment trapping capability ($2.2 \sim 4.4$ times) under lower coverage and rainfall intensity than erect grass, even under high rainfall intensity ($1.1 \sim 3.2$ times). The stolon grass played more beneficial roles in soil and water conservation than erect grass, which was closely related to above-ground and under-ground parts of grass. This study can provide a better understanding of the roles of stolon and erect grass species for soil and water conservation and management practices.

1. Introduction

Soil erosion is a severe eco-environmental concern that leads to the loss of soil organic matter, fertility and nutrients, thus causing the disruption of soil aggregates and affecting agricultural productivity, particularly in the increasing frequency of extreme rainfall events (Sadeghi et al., 2020; Li et al., 2021). The soil erosion problems in the southern hilly region of China were caused by the interactions of high

precipitation, fragmented topography, and intensive agricultural activities (Liu et al., 2016a; Jiang et al., 2018; Duan et al., 2022). Vegetation plays a dominant role in alleviating soil erosion and regulating the relationship between runoff and sediment, which is a widely adopted measure on hillslopes worldwide (Wuepper et al., 2019).

Previous research has been conducted to analyze the effects of grass on overland flow and soil erosion processes (Pan et al., 2016; Zhang et al., 2022), and the results reveal that the grass cover is effective in

* Corresponding author at: School of Geographic Sciences, Hunan Normal University, Changsha, 410081, China.

E-mail address: liuyj461@163.com (Y. Liu).

reducing runoff and sediment generation and increasing surface roughness (Zhang et al., 2018; Duan et al., 2022). Pan et al. (2006) proposed that grass had more significant roles in sediment concentration than in surface runoff; and the sediment reductions ranged from 45 % to 85 % on the Loess Plateau. Fattet et al. (2011) indicated that grass was more conducive to soil aggregate stability and anti-erosion than other vegetation types such as trees. Li and Pan (2018) suggested that grass significantly reduced overland flow rate and velocity and sediment generation, with average reductions of 22 %, 29 % and 67 %, respectively. Sun et al. (2019) suggested that grass coverage could significantly affect runoff shear stress and sediment transport capacity by reducing the splash energy of raindrops. Many studies have also demonstrated that grass had important effects on facilitating water infiltration and improving the topsoil physical property (Tu et al., 2021; Zhang et al., 2022). Furthermore, grass has been known to help moderate extreme rainfall and balance water for farming, which presents the advantages of reducing the rapid response of surface flow to extreme climate and safeguarding subsurface reservoirs (Li et al., 2009; Duan et al., 2022). Therefore, it is essential to utilize grass reasonably to reduce fluxes of eroding soil and regulate the relationship between runoff and sediment.

Distinct response of runoff and sediment processes appeared among different grass species (Zheng et al., 2008; Wei et al., 2014). El Kateb et al. (2013) highlighted the necessity of selecting suitable grass species for the region to maximize its water and soil control efficiency. Similar findings were also reported by Li et al. (2015) and Duan et al. (2016) that the grass species was the most significant factor affecting the frequency and intensity of soil loss. A comparison on three grass species conducted by Hatefi et al. (2020) found that *L. perenne* performed best in controlling runoff and soil loss compared with *Agropyron trichophorum* and *Medicago sativa* from on small experimental plots. Duan et al. (2022) demonstrated that the effects of three grass species (*Trifolium repens*, *Cynodon dactylon* and *Eremochloa ophiuroides*) on runoff, hydrodynamic parameters and sediment reductions were evidently different.

Exploring the roles of grass components (stems, leaves and roots, etc.) on soil erosion has been shown to be meaningful for soil erosion control (Li and Pan, 2018; Li et al., 2021; Wang et al., 2021a,b). Grass canopies increase water infiltration and reduce water hydraulic shear by intercepting rainfall (Zhang et al., 2020). The grass roots can consolidate soil aggregate, improve soil structure and reduce soil erosion (Wang et al., 2021a). Inconsistent results regarding the effects of the above-ground and under-ground parts of grass on erosion-controlling benefits exist. De Baets et al. (2007) highlighted the above-ground parts of grass could be considered as a key factor for reducing water erosion and increasing the surface resistance. Zhou and Shangguan (2007) demonstrated that ryegrass could enhance the soil aggregate stability; and the above-ground parts contributed relatively more to reducing runoff, while the root effect on soil loss reduction was greater than the shoot effect. Sadeghi et al. (2017) scientifically proved that canopy can promote the formation of stemflow in favor of the water supply to roots, thereby changing the redistribution of water in soil. Furthermore, an experiment conducted by Wang et al. (2021a) found that the root morphology traits of grass species can determine the soil detachment process, especially the root surface area density.

Grass density is recognized as a crucial factor in affecting soil and water conservation benefits of grass (Wei et al., 2014; Duan et al., 2022). The reasonable grass density can effectively improve rainfall interception, alter rill erosion and gully erosion (Fattet et al., 2011; Tong et al., 2018). Grass cover thresholds vary significantly in different climates and soils, so the effective grass coverage needs to be site-specific. Additionally, frequent extreme rainfall events need more attention, which exerted disproportionate impacts on the relationship between runoff and sediment (Wei et al., 2014; Pan et al., 2019; Zhang et al., 2022). The increase in extreme rainfall events possibly poses a significant threat to achieving sustainable water management (Wang et al., 2020). Therefore, studying different grass measures under heavy rainfall has practical implications for soil and water conservation.

Hydraulic and hydrodynamic parameters which can indicate the mechanism of grass planting in water and soil erosion should be quantified (Jiang et al., 2018; Li et al., 2021). Many studies have demonstrated that grass canopies and roots can decrease flow velocity (v), Froude number (Fr), flow shear stress (τ) and stream power (ω), increase the hydraulic resistance, and weaken the kinetic energy (Pan et al., 2016; Zhang et al., 2020; Jafarpoor et al., 2022). Waldron and Dakessian (1981) and Wang et al. (2021a) indicated that the primary factors affecting these characteristics of runoff included the morphology and distribution of grass roots in soil. Jiang et al. (2018) reported that the rill flow velocity was the most sensitive hydraulic parameter, and the flow power provided the optimal hydrodynamic parameter to characterize the dynamic mechanisms of soil erosion. Zhang et al. (2020) explored the effects of canopies and root systems of two grasses (*M. minutiflora* and *C. zizanioides*), and found they effectively decreased flow velocities (v) by 35 % and 30 %, and increased Darcy–Weisbach friction coefficients (f) by 240 % and 131 % compared to the control treatments, respectively. However, the effects of grass species on the hydraulic and hydrodynamic processes still need to be supplemented by subsequent in-depth research (Wei et al., 2014; Li et al., 2021).

Numerous studies mainly focus on the effects of grass species from the perspective of surface flow or sediments, while ignoring its impact on subsurface flow generation, especially for red soil (Zhou and Shangguan, 2007; El Kateb et al., 2013; Wang et al., 2021b). Red soil hilly regions are subject to high temperature, concentrated precipitation and some unreasonable farming activities, resulting in serious water and soil loss. The red tillage soil is mainly composed of a loose, porous and highly permeable top layer while a compact and weakly permeable bottom layer (Ma et al., 2022), which facilitates the lateral flow of runoff after infiltration to form subsurface flow (Liu et al., 2016b). The soil covered by dense grass can significantly increase the soil infiltration and promote the subsurface flow generation. Zheng et al. (2014) indicated that subsurface flow accounted for 52 %–68 % of the total runoff on red soil sloping farmland through simulated laboratory rainfall experiments. Nespolous et al. (2019) proposed grass diversity and their fine roots were significant for promoting the incidence of subsurface flow, thus reducing water and soil erosion in tropical Ferralsols. While the roles of stolon and erect grass species on surface–subsurface flow are still unclear.

In this study, two common native grass species, *E. ophiuroides* (stolon type) and *L. perenne* (erect type) were selected in the rainfall simulation experiment. They were widely used in ecological restoration in the red soil hilly region of South China owing to their rapid growth, strong tillering ability, and large biomass. The study objectives were to identify the roles of stolon and erect grass species on the spatial vertical distribution of surface flow and subsurface flow, test the efficiencies of two grass species on sediment trapping, and reveal the soil erosion mechanisms from the perspective of hydraulics and hydrodynamics. The results can provide references for guiding the choice of grass species for soil and water conservation.

2. Materials and experimental methods

2.1. Study area and experimental soil

The study area is located in the Soil and Water Conservation Ecological Technology Park in the De'an county of Jiangxi Province, approximately between 29°14'–29°29' N and 115°32'–115°45' E, in the southern hilly region of China. Rugged hills and low mountains comprise this region. The soil parent material is dominated by Quaternary sediment and featured by the high erodibility (Cao et al., 2015; Zhang et al., 2022). Over 70 % of the total annual precipitation primarily occurs between March and July, mainly due to its subtropical monsoon climate. The sloping farmland is the main land use type in the hilly red soil region; meanwhile, the high intensity sloping farmland cultivation coincided with the high intensity rainfall contributes more

than half of soil erosion during the rainy season.

The experimental soil was collected from the 0–30 cm layer of the long-term cultivated sloping farmland. The soil texture was silty clay, with clay (<0.002 mm), silt (0.002–0.05 mm), and sand (0.05–2 mm) contents being 26.8 %, 61.8 %, and 11.4 %, respectively, according to the United States Department of Agriculture classification standards. The basic physical and chemical properties of the experimental soil were shown in Table 1. Soil organic matter content (OM) was measured by the Walkley-Black wet oxidation method and potassium permanganate oxidation method, total nitrogen (TN) was identified by the Kjel-dahl method, total phosphorus (TP) was determined by the molybdenum blue colorimetric method, cation exchange capacity (CEC) was measured on the fine earth fraction, pH was measured by PHS-3C pH meters at a 1:2.5 soil to water ratio, and Free iron oxide (Fed) was extracted by sodium dithionite-citrate-bicarbonate treatment method (ISSAS, 1978).

2.2. Soil plot design and installation

The soil plots were constructed of iron and steel plates in three replicates with the size of 2 m long, 0.5 m wide, and 0.5 m deep (Fig. 1). This small scale plot can simplify the process and minimize the uncertainties in a relatively homogeneous slope surface, thereby excluding confounding factors other than vegetation (Sadeghi et al., 2016; Wang et al., 2021b). The experiment was conducted at a slope gradient of approximately 10° (18 %) to simulate the typical gradient of the sloping farmland in the hilly red soil region (Liu et al., 2016a,b; Duan et al., 2022). The soil was filled into the plot and compacted in every 5 cm layers, and the soil used in each 5 cm layer was weighed to ensure the soil bulk density were compacted at 1.3 g cm⁻³. An upper outlet flush with topsoil was installed to collect the surface flow and sediment during the rainfall simulation, and a lower outlet flush with the bottom of the soil plot was set up to collect the subsurface flow. The outlet of the subsurface flow was set at a soil depth of 0.5 m, which was collected into the flow storage container by a pipe connected to a hole that in the L-type subsurface flow collector (Liu et al. 2016b). Uniform small holes were arranged at the bottom of the soil plot to ensure that the water could flow freely downward. The percolating water was collected by a plate that was set beneath the soil plot bottom. Before planting the studied grass on the plots, artificial surface levelling was undertaken to minimize the impact of microtopographic changes (Li and Pan, 2018).

2.3. Grass planting and management

Two kinds of common native grasses (*E. ophiuroides* and *L. perenne*) were employed in this study, which can function for soil and water conservation after 3–5 months growth (Li et al., 2021). *E. ophiuroides* is a perennial warm season grass with approximately 20 cm height and well-developed strong stolons. The fast-growing perennial *L. perenne* is suitable for the warm and humid climate which has skinny and supple erect stems with approximately 30–90 cm heights. Three surface coverage gradients were set: a bare soil plot (BSP) as the control; EC30 (LC30) and EC70 (LC70) represent *E. ophiuroides* (*L. perenne*) plots with 30 % and 70 % coverage, respectively. The two grass species were strip sowed on the soil plots and then managed by regular watering and fertilization until the desired coverage was achieved (Zhang et al., 2018). Once the grass coverage requirements (30 % and 70 %) were met by digital image analysis, the simulated rainfall tests were initiated. The no grass (NG)

plots were treated to the same watering and fertilization conditions as the grass-covered plots. All treatments were replicated thrice with complete combinations of coverage and rainfall intensity.

2.4. Rainfall simulation

The rainfall simulator was composed of a water source, pipeline pump, rainfall control cabinet, rain shelter, and a SPRACO cone jet nozzle (Liu et al., 2016b). The rainfall process was computer-operated, and supported by manual operation. The rainfall intensity was adjusted by regulating the water pressure of the pump and nozzle sizes, which could range from 10 to 300 mm h⁻¹. The height of the rainfall simulator was 22.4 m, so that the final raindrop speed was similar to that of the natural rainfall before it reached the soil surface. The simulated raindrops were produced by two opposite nozzles. Before each rainfall simulation, several rainfall collection buckets were set up within the effective rainfall range with a density of 20 × 20 cm, and the uniformity of the simulated rainfall device was calculated at a 10 min rainfall with intensity of 60 mm h⁻¹ under 5 times repetitions, and the rainfall uniformity coefficient was more than 85 %. In this study, the representative erosive rainfall intensities (60 and 120 mm h⁻¹) were conducted, considering the high-intensity and short-duration rainstorms that occur in the humid hilly region of South China, respectively (Liu et al., 2016a; Zhang et al., 2020). Prior to the simulation, calibrations of the rainfall intensity and uniformity were conducted. The test plot was pre-wetted with a low intensity rainfall (10 mm h⁻¹) to eliminate the difference in antecedent soil moisture (Cao et al., 2015); and prior surface levelling was undertaken to minimize differences in microtopographic variations (Jiang et al., 2018; Li and Pan, 2018). Through these measures, the micro-topography, early soil moisture and dry bulk weight of the whole block were basically the same before each experiment.

Rainfall simulations were conducted with 90-minute duration. During each simulated rainfall event, the initial generation time of surface and subsurface flow were recorded, three bottles (200 mL for each) of water mixed with sediment samples were collected at 3-minute intervals, and then the mixed samples were oven dried at 105 °C for 24 h and weighed to determine the sediment concentration and soil loss rate. The surface flow velocity was measured by a KMnO₄ solution coloration at 15-minute intervals after rainfall simulation, and each measure interval was repeated four times. Simultaneously, three bottles of 100 mL mixed water and sediment samples were collected to test the eroded sediment particle size. The sediment samples were analyzed by the Malvern Mastersizer 2000 laser diffraction device (Malvern Instruments Ltd., UK). The instrument's agitator speed was 2500 r min⁻¹, and the range of shading and measurement were 20 %–30 % and 0.01–2000 μm, respectively (Liu et al., 2016a). Each sample was transferred to the fluid module that contained 1.7 L of deionized water (20 °C) and then subjected to three consecutive 1-minute runs at a pump speed of 8 to 12 L min⁻¹ (Shi et al., 2013), and the particle diameter of the total cumulative sediment particles of 50 % (D₅₀) were calculated. The sediment particle sizes under different treatments were compared based on sediment median size (D₅₀) (Sadeghi et al., 2018). When the rainfall simulation was complete, a lagged subsurface flow was collected to calculate its total generation amount.

2.5. Data collection and analysis

To explore the hydraulic and hydrodynamic characteristics of the

Table 1

Summary of the basic physical and chemical properties of the experimental soil.

Coarse sand / (g·kg ⁻¹)	Fine sand / (g·kg ⁻¹)	Coarse silt / (g·kg ⁻¹)	Fine silt / (g·kg ⁻¹)	Clay / (g·kg ⁻¹)	OM / (g·kg ⁻¹)	TN / (g·kg ⁻¹)	TP / (g·kg ⁻¹)	CEC / (mol·kg ⁻¹)	pH	Fed / (mg·kg ⁻¹)
75.1 ± 21.8	171.7 ± 39.7	198.9 ± 7.3	332.4 ± 12.4	221.9 ± 29.1	11.0 ± 1.6	0.9 ± 0.1	0.2 ± 0.1	19.3 ± 3.3	4.3 ± 0.1	41.2 ± 6.0

OM = Organic matter, TN = Total nitrogen, TP = Total phosphorus, CEC = Cation exchange capacity, Fed = Free iron oxide.

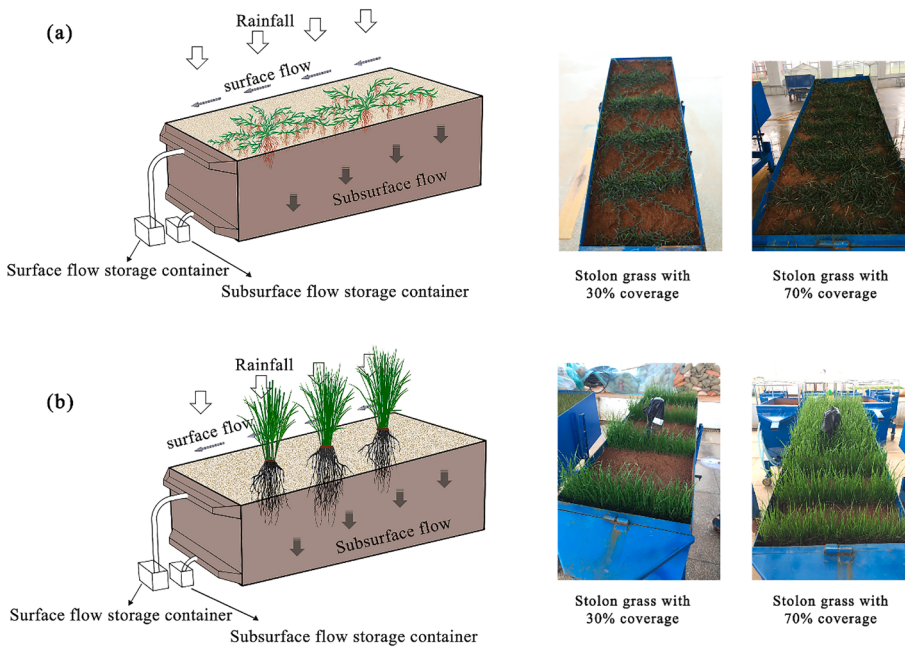


Fig. 1. Schematic diagram of soil plots and grass species used in the experiment. (a) *E. ophiuroides*, (b) *L. perenne*.

flow under different grass treatments, Reynolds number, Froude number, Darcy–Weisbach friction coefficient, Manning friction coefficient, flow shear force, and stream power were analyzed.

The Reynolds number (Re) is defined as the ratio of fluid inertial to viscous forces; the formula is as follows (Jafarpoor et al., 2022):

$$Re = \frac{vh}{U} \quad (1)$$

where v is the mean velocity (m/s), h is the flow depth (m), and U is the water viscosity coefficient, whose value is 7.0×10^{-5} m²/s. The mean flow depth (h) can be calculated by using the equation (Zhang et al., 2020):

$$h = \frac{q}{v} = \frac{Q}{Bvt} \quad (2)$$

where q represents the unit flow discharge (m³/s), Q refers to the total flow volume (m³) during time t (s), and B is the width of water-crossing section (m).

The Froude number (Fr) is a dimensionless parameter that represents the ratio of the inertial to gravitational forces. It is calculated as follows (Pan and Shangguan, 2006):

$$Fr = \frac{U}{\sqrt{gh}} \quad (3)$$

where g refers to the mean acceleration of gravity (m s⁻²).

The Darcy–Weisbach coefficient (f) and Manning friction coefficient (n) can be used to describe the resistance to overland flow from soil (Jiang et al., 2018). The formulas are as follows:

$$f = \frac{8ghJ}{v^2} \quad (4)$$

$$n = \frac{R^{2/3}}{v} \quad (5)$$

where J is the hydraulic energy slope which is estimated by cosine of the slope ($\cos \theta$, m m⁻¹), and R is hydraulic radius.

The flow shear stress (τ) reflects the degree of the erosion force for destroying the soil structure and separating soil particles when the runoff flows (N/m²(-|J|)). The formula is calculated as follows (Zhang

et al., 2020):

$$\tau = \rho ghJ \quad (6)$$

where ρ refers to the water density (g cm⁻³).

The stream power (w) is applied to describe the influence of rainfall on the hydrodynamic mechanism of soil erosion (J m⁻² s⁻¹). It is calculated using the following formula (Wang et al., 2018; Zhang et al., 2020):

$$w = \tau v = \rho g J Q \quad (7)$$

The Pearson correlation analysis was conducted to describe the relationships between surface–subsurface flow, sediment concentration and hydraulic–hydrodynamic parameters. P value was <0.05 for significant difference.

3. Results

3.1. Surface flow generation

The grass significantly decreased the surface flow coefficient, and the effect of two grass species in surface flow generation differed more significantly under lower rainfall intensity (Fig. 2). When the rainfall intensity was 60 mm h⁻¹ (RI₆₀), the average surface flow coefficient on bare soil was 58.8 %, while the values sharply decreased to 42.1 % on LC30 and 30.0 % on LC70, with values of 17.1 % on EC30 and 12.5 % on EC70 (Table 2). The ratios of bare soil surface flow coefficient divided by the values of grass treatments ranged from 1.4 to 4.7. For the 120 mm h⁻¹ rainfall intensity (RI₁₂₀), the ratios became lower with values ranging from 1.1 to 1.3. Particularly, the average surface flow coefficient of BSP was 88.2 %, while those of LC30 and LC70 were 83.1 % and 72.5 %, and those of EC30 and EC70 were 80.0 % and 69.4 %, respectively.

3.2. Subsurface flow generation

The subsurface flow of the grass-covered plots was higher than that of the BSP (Table 3). The BSP displayed the lowest average subsurface flow coefficient, with values ranging from 4.8 % to 13.0 % under RI₆₀ and from 1.0 % to 5.5 % under RI₁₂₀. Furthermore, the lowest mean

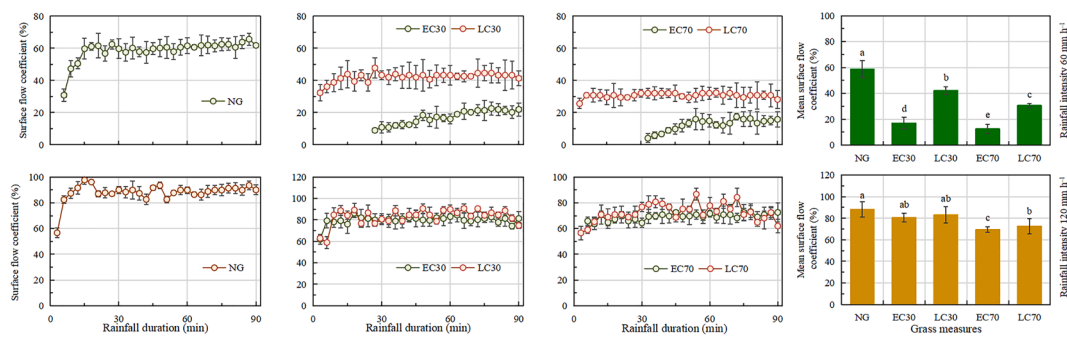


Fig. 2. Surface flow coefficients combination chart of different grass species, grass coverage and rainfall intensities. Values with superscript letters (a–e) are significantly different across columns at the $\alpha = 0.05$ level using the least significant difference (LSD) analyses.

Table 2
Characteristics of surface flow (SF) under different grass measures.

Grass measures	60 mm h ⁻¹					120 mm h ⁻¹				
	NG	EC30	EC70	LC30	LC70	NG	EC30	EC70	LC30	LC70
Initial generation time (min)	6	27	33	3	3	3	3	6	3	3
Peak volume of SF (L)	1.1	0.4	0.3	1.9	1.3	4.9	4.9	4.1	4.6	4.4
Mean volume of SF (L)	1.0	0.3	0.2	1.6	1.2	4.5	4.5	3.9	4.2	3.7
Peak value of SF coefficient (%)	65.6	22.5	17.4	47.7	32.2	97.7	86.4	73.3	90.7	86.7
Mean value of SF coefficient (%) \pm SD	58.8 \pm 6.4a	17.1 \pm 4.3d	12.5 \pm 3.7e	42.1 \pm 2.8b	30.7 \pm 1.4c	88.2 \pm 6.8a	80.0 \pm 4.0ab	69.4 \pm 2.5c	83.1 \pm 7.4ab	72.5 \pm 6.8b

Note: SD refers to standard deviation; Values with superscript letters (a–e) are significantly different across columns at the $\alpha = 0.05$ level using the least significant difference (LSD) analyses.

Table 3
Characteristics of subsurface flow (SSF) under different grass measures.

Grass measures	60 mm h ⁻¹					120 mm h ⁻¹				
	NG	EC30	EC70	LC30	LC70	NG	EC30	EC70	LC30	LC70
Initial generation time (min)	39	15	18	42	33	27	36	24	27	9
Peak volume of SSF (L)	0.2	0.6	1.0	0.3	0.4	0.3	0.8	1.2	0.4	0.6
Mean volume of SSF (L)	0.2	0.5	0.8	0.2	0.4	0.2	0.5	0.9	0.3	0.5
Peak value of SSF coefficient (%)	13.0	35.8	60.2	17.5	26.1	5.5	13.4	21.2	6.9	11.5
Mean value of SSF coefficient (%) \pm SD	11.0 \pm 1.9d	28.7 \pm 3.8b	48.7 \pm 11.1a	12.8 \pm 3.6d	23.3 \pm 3.4c	3.4 \pm 1.5e	8.6 \pm 3.0c	16.5 \pm 4.1a	5.8 \pm 1.3d	10.2 \pm 1.4b

subsurface flow was 185 mL (RI₆₀) and 172 mL (RI₁₂₀) with poor vegetation cover conditions on the BSP, followed by LC30, with values of 216 mL (RI₆₀) and 293 mL (RI₁₂₀).

The subsurface flow initial generation (mean 27 min) took more time than the surface flow (mean 8 min). Fig. 3 shows the subsurface flow coefficient of the entire duration in the experimental process. Compared to the *L. perenne* plots, the *E. ophiuroides* plots contributed more to increasing the subsurface flow. The mean subsurface flow coefficients were 28.7 % on EC30 and 48.7 % on EC70 under RI₆₀, which were 20.1

% and 32.2 % larger than those on LC30 and LC70, respectively. For the RI₁₂₀, the *L. perenne* plots produced slightly more subsurface flow than the *E. ophiuroides* plots during the early stage, with LC30 and LC70 starting to be lower than EC30 and EC70 after 48 and 30 min, respectively. Eventually, with the increase in the rainfall duration, the fluctuation of subsurface flow in each experimental plot stabilized.

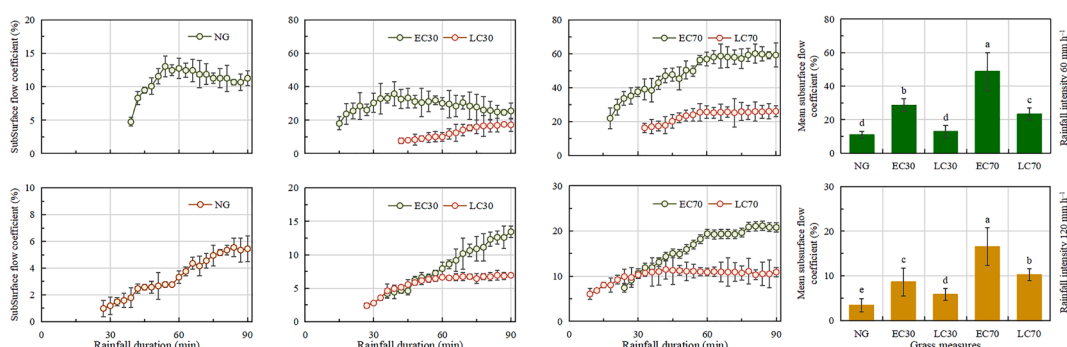


Fig. 3. Subsurface flow coefficients combination chart of different grass species, grass coverage and rainfall intensities.

3.3. Sediment yield

The influence of different land cover types on the sediment yield is shown in Table 4. The mean value of sediment concentration and soil loss rate generally decreased with increasing coverage. The BSP had the higher mean sediment concentration, with values of 6.0 and 4.9 times higher than *E. ophiurooides* and *L. perenne*, respectively. Similarly, the highest mean soil loss rate occurred on the BSP, with values of $4.3 \text{ g m}^{-2} \text{ min}^{-1}$ under RI₆₀ and $17.1 \text{ g m}^{-2} \text{ min}^{-1}$ under RI₁₂₀.

The soil loss rate on *E. ophiurooides* plots was less than that on *L. perenne* plots (Fig. 4). EC30 contributed more to reducing the soil loss rate, with mean values of 0.4 and $1.8 \text{ g m}^{-2} \text{ min}^{-1}$ for RI₆₀ and RI₁₂₀, which were 4.0 and 3.2 times lower than those observed for LC30, respectively. Moreover, LC70 had a higher soil loss rate than EC70, with an average of 0.4 and $2.1 \text{ g m}^{-2} \text{ min}^{-1}$ for RI₆₀ and RI₁₂₀, respectively, the values being 4.0 and 2.3 times higher than those recorded for the *E. ophiurooides* plots. Furthermore, the generation time of the sediment yield on *E. ophiurooides* plots was relatively later than on other land cover types under RI₆₀, with values of 27 min on 30 % cover and 33 min on 70 % cover. The standard deviations of the soil loss rate for BSP were significantly higher than that for the grass-covered plots. Once the plots were covered with grass, the values of these standard deviations fell below 1.0.

3.4. Hydraulic and hydrodynamic characteristics

The flow velocity decreased with the increase in grass coverage. As shown in Table 5, the flow velocity reached its maximum on the BSP, with values being 6.1×10^{-2} and 9.4×10^{-2} m/s under RI₆₀ and RI₁₂₀, respectively. The mean v decreased from 2.5×10^{-2} to 2.3×10^{-2} m/s during RI₆₀ and from 3.4×10^{-2} to 2.8×10^{-2} m/s during RI₁₂₀, when the coverage increased from 30 % to 70 % for the *E. ophiurooides* plots. The similar variation trend was observed for the *L. perenne* plots. In addition, *E. ophiurooides* was more effective in reducing the flow velocity than *L. perenne*. For example, when the rainfall was 60 mm h^{-1} , the mean v on EC30 was 1.8×10^{-2} m/s lower than that on LC30, and that on EC70 was 1.6×10^{-2} m/s lower than that on LC70.

The significance statistics showed that mean Re increased from 10.62 (RI₆₀) to 51.52 (RI₁₂₀) with the increase of rainfall intensity (Table 6). The lower coverage of grass plots led to relatively higher Re . The mean Re of *E. ophiurooides* plots decreased from 3.58 to 2.63 as the coverage increased from 30 % to 70 % under RI₆₀, and that of *L. perenne* plots declined from 20.26 to 14.74 under the same conditions. The Re for EC30 and LC30 was 56.15 and 52.08 under RI₁₂₀, with mean values of 7.52 and 6.64 higher than EC70 and LC70, respectively. In addition, Re ranged from 0.84 to 56.16 for all treatments, which suggested that the experimental overland flows were regarded as laminar flows ($Re < 500$) according to the open channel standard. Fr for the BSP kept ranged from 1.24 to 2.01, being the highest when compared to the grass-covered plots ($Fr < 1$), with mean values of 1.41 (RI₆₀) and 1.31 (RI₁₂₀). The lowest mean value of f was found for the BSP, ranging from 11.25 to 23.99 during RI₆₀ and from 17.03 to 29.38 during RI₁₂₀. Similarly, the f for the *E. ophiurooides* plots for 70 % cover was 930.43 under RI₁₂₀, with

values of 351.78 higher than that for 30 % cover; the f for the *L. perenne* plots varied very little from 128.02 to 126.39, respectively. The lowest n was recorded for the BSP, with mean values of 0.12 (RI₆₀) and 0.17 (RI₁₂₀).

There was a slight shift in mean τ from 2.41 to 9.82 N m^{-2} during RI₆₀, while a sharper fluctuation was observed under RI₁₂₀ ranging from 12.25 to 36.82 N m^{-2} . Statistical analysis showed that the *E. ophiurooides* plots had the lowest mean τ amongst the plots, with an average value of 2.94 N m^{-2} on EC30 and 2.41 N m^{-2} on EC70 under RI₆₀. With regard to w , the mean values for the *L. perenne* plots were 0.42 and $0.31 \text{ J m}^{-2} \text{ s}^{-1}$ for low and high coverage during RI₆₀, which were approximately 5.66 and 5.60 times more than the corresponding values for the *E. ophiurooides* plots.

3.5. Correlation analysis

As shown in Fig. 5, the surface flow had positive relations with some hydraulic and hydrodynamic parameters ($p < 0.05$), with the correlation coefficients in the descending order of $Re > \omega > \tau > f > n > v$. This indicated that flow regimes had considerable effects on overland flow generation. Additionally, the w has a stronger correlation with the surface flow compared with the τ . The subsurface flow showed a significantly negative relationship with v and SC, which can reflect soil erosion and sediment yield. The movement of sediment is based on runoff as the driving force, thereby the hydraulic and hydrodynamic parameter of runoff profoundly affected the sediment transportation. The velocity is a crucial hydraulic parameter influencing sediment transport capacity. Specifically, the sediment concentration was positively correlated with v and Fr , whereas it decreased with increasing values of f , n and τ . The f was expected to increase with the increments of n and τ . In contrast with velocity, Re and w were poor predictors for sediment concentration. Generally, the correlation of each hydraulic and hydrodynamic parameter was mainly dependent on grass species, soil property, rainfall intensity, and surface roughness. The combination of multiple hydraulic and hydrodynamic parameters can lead to more rational and scientific analysis of soil and water erosion process.

4. Discussion

4.1. Effects of grass species on runoff components

In this study, the maximum distribution proportion of the surface flow (more than 15.0 %) and the minimum subsurface flow (<2.0 %) were observed for the BSP. When the *L. perenne* plots were exposed to RI₆₀, the increment of coverage increased the subsurface flow rate from 2.0 % to 4.4 % and decreased the surface flow rate from 27.2 % to 19.9 %; similar observations were recorded for the *E. ophiurooides* plots. The conclusion aligned with the finding of Zhou and Shangguan (2007), who explained that the contribution of grass canopy to runoff reduction performed best for *L. perenne* plots based on rainfall simulation. The above-ground parts of grass could reduce soil temperatures and evaporation by shading the soil surface, thus improving soil water storage capacity (Zhang et al., 2022). Furthermore, grass could form root

Table 4
Characteristics of sediment yield under different grass measures.

Grass measures	60 mm h ⁻¹					120 mm h ⁻¹				
	NG	EC30	EC70	LC30	LC70	NG	EC30	EC70	LC30	LC70
Initial generation time (min)	6	27	33	3	3	3	3	6	3	3
Peak value of sediment concentration (g L ⁻¹)	22	5	3	3	3	14	1	1	5	2
Mean value of sediment concentration (g L ⁻¹)	10	3	2	2	1	9	1	1	3	1
Peak value of soil loss rate (g m ⁻² min ⁻¹)	9.9	0.5	0.3	2.4	1.2	31.0	2.8	1.5	8.8	4.0
Mean value of soil loss rate (g m ⁻² min ⁻¹) ± SD	$4.3 \pm 2.8a$	$0.4 \pm 0.1c$	$0.1 \pm 0.0d$	$1.6 \pm 0.4b$	$0.3 \pm 0.3c$	$17.1 \pm 6.2a$	$1.8 \pm 0.4d$	$0.9 \pm 0.3e$	$5.7 \pm 1.3b$	$2.1 \pm 0.7c$

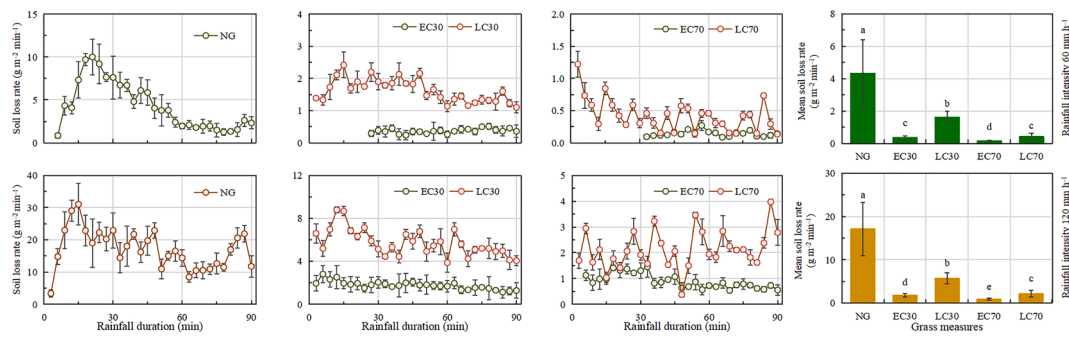


Fig. 4. Soil loss rates combination chart of different grass species, grass coverage and rainfall intensities.

Table 5
Variation of flow velocity (cm/s) during rainfall tests at 15 min interval.

Flow velocity tested time	60 mm h ⁻¹					120 mm h ⁻¹				
	NG	EC30	EC70	LC30	LC70	NG	EC30	EC70	LC30	LC70
15 min	6.4 ± 0.5a	2.3 ± 0.1c	2.2 ± 0.1c	4.7 ± 0.4b	4.3 ± 0.4b	10.3 ± 1.8a	3.1 ± 0.1c	2.7 ± 0.1c	5.2 ± 0.6b	4.6 ± 0.5bc
30 min	5.4 ± 0.4a	2.7 ± 0.3c	2.1 ± 0.2c	4.5 ± 0.6b	4.0 ± 0.3b	12.7 ± 0.7a	3.3 ± 0.2c	3.2 ± 0.2c	5.4 ± 0.4b	5.8 ± 0.4b
45 min	6.4 ± 0.8a	2.4 ± 0.2c	2.4 ± 0.1c	3.9 ± 0.4b	3.6 ± 0.3b	7.6 ± 2.0a	3.8 ± 0.3bc	2.5 ± 0.1c	5.0 ± 0.5b	5.4 ± 0.3b
60 min	6.8 ± 0.8a	2.5 ± 0.2c	2.5 ± 0.1c	4.4 ± 0.2b	3.8 ± 0.2b	8.7 ± 0.4a	3.2 ± 0.1d	2.9 ± 0.2d	5.8 ± 0.3b	5.0 ± 0.3c
75 min	5.9 ± 0.5a	2.9 ± 0.3c	2.2 ± 0.1c	4.1 ± 0.2b	3.6 ± 0.2b	9.2 ± 2.0a	3.7 ± 0.5c	2.6 ± 0.1c	6.1 ± 0.8b	5.6 ± 0.5bc
Total mean	6.2 ± 0.8a	2.6 ± 0.3d	2.2 ± 0.2d	4.3 ± 0.5b	3.8 ± 0.4c	9.6 ± 2.3a	3.4 ± 0.4c	2.8 ± 0.3c	5.9 ± 0.7b	5.2 ± 0.6b

Table 6
Mean values of hydraulic and hydrodynamic parameters under different grass measures.

Hydraulic and hydrodynamic parameters	60 mm h ⁻¹					120 mm h ⁻¹				
	NG	EC30	EC70	LC30	LC70	NG	EC30	EC70	LC30	LC70
<i>Re</i>	11.91 ± 0.27c	3.58 ± 1.66d	2.63 ± 1.62e	20.26 ± 0.46a	14.74 ± 0.68b	55.31 ± 2.10a	56.15 ± 1.86a	48.63 ± 2.96c	52.08 ± 2.04b	45.44 ± 3.98c
<i>Fr</i>	1.41 ± 0.20a	0.74 ± 0.37b	0.75 ± 0.42b	0.67 ± 0.07b	0.66 ± 0.08b	1.31 ± 0.41a	0.28 ± 0.03c	0.22 ± 0.04c	0.60 ± 0.07b	0.60 ± 0.07b
<i>f</i>	21.49 ± 26.18c	87.26 ± 93.09b	89.53 ± 121.83b	101.40 ± 63.20a	105.20 ± 63.66a	26.51 ± 94.53d	578.66 ± 298.13b	930.43 ± 557.69a	128.02 ± 110.44c	126.39 ± 102.57c
<i>n</i>	0.12 ± 0.02c	0.23 ± 0.10b	0.23 ± 0.13bc	0.31 ± 0.04a	0.31 ± 0.04a	0.17 ± 0.05d	0.92 ± 0.12b	1.18 ± 0.21a	0.39 ± 0.21a	0.38 ± 0.05c
<i>τ</i>	4.20 ± 0.41c	2.94 ± 1.28d	2.41 ± 1.46e	9.81 ± 0.67a	8.03 ± 0.75b	12.25 ± 2.35d	34.59 ± 2.60a	36.82 ± 4.99a	19.90 ± 1.59b	18.09 ± 1.38c
<i>w</i>	0.26 ± 0.01c	0.07 ± 0.03d	0.05 ± 0.03e	0.42 ± 0.01a	0.31 ± 0.01b	1.15 ± 0.04a	1.17 ± 0.04a	1.01 ± 0.06c	1.08 ± 0.04b	0.95 ± 0.08c

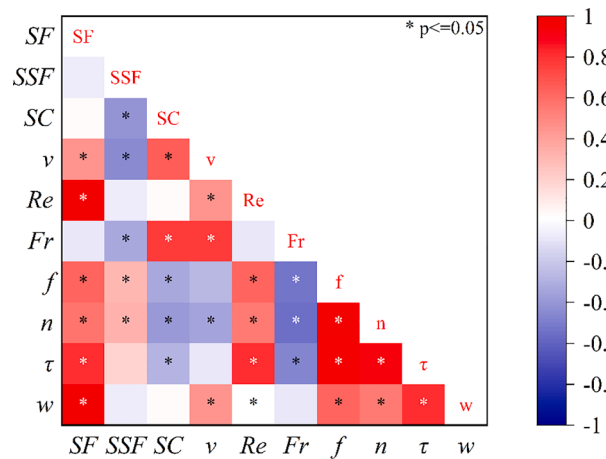


Fig. 5. Correlation analysis of surface flow (SF), subsurface flow (SSF), sediment concentration (SC), hydraulic and hydrodynamic parameters (*v*: velocity, *Re*: Reynolds number, *Fr*: Froude number, *f*: Darcy-Weisbach friction coefficient, *n*: Manning friction coefficient, *τ*: flow shear force, *w*: stream power).

channels which facilitate water entry, increase soil porosity and infiltration.

Stolon and erect grass species played various roles in surface-subsurface flow generation by affecting the rainfall redistribution (Zhang et al., 2018; Tu et al., 2021). *E. ophiuroides* accounted for less proportion of surface flow (18.8 %) and more proportion of subsurface flow (6.7 %), with mean values of 9.3 % lower and 3.1 % higher than the *L. perenne* plots, respectively. In addition, the proportion of surface flow was significantly larger than that of the subsurface flow, except for the *E. ophiuroides* plot under RI₆₀ in this study, whose subsurface flow accounted for 7.0 % and 11.4 % for 30 % and 70 % coverage, the values being 3.5 % and 9.1 % larger than those of the surface flow, respectively. The runoff interception efficiency of *E. ophiuroides* was the highest, reaching 72.0 % at low cover and 79.0 % at high cover. These results above indicated stolon grass had higher water retention capacity to regulate rainfall-runoff relationship compared to erect grass (Wei et al., 2014). This is probably owing to different mulching patterns and morphology of stolon and erect grass. The stolons of *E. ophiuroides* spread out in all directions and formed a net-like structure, thus gradually reducing the flow velocity, increasing flow tortuosity and providing sufficient time for infiltration (Li and Pan, 2018; Li et al., 2021; Wang et al., 2021b). Local investigation in South China found that

L. perenne has a higher stalk height than *E. ophiurooides*. The higher leaves and cluster stems of the *L. perenne* above-ground caused a higher significant rainfall interception. However, the shorter but stronger spread ability of the stolon grass could easily receive a higher surface coverage, which was more crucial in reducing soil crust formation (Gao et al., 2017; Digiovanni-White et al., 2018). Once the soil crust existed, more and faster surface flow generated, and this more important under the higher rainfall intensity (Gómez and Nearing, 2005). Besides, the erect grass had a relatively weaker impact in retaining and intercepting rainfall due to its tender canopies and thin leaves (Li et al., 2021; Wang et al. 2021b). Zhou and Shangguan (2007) also proposed that soil infiltration rate had linear correlation with root density. Based on field investigation and literature, the *E. ophiurooides* formed dense fine root networks, which played a predominant role in retaining rainfall, altering the distribution of raindrops, and enhancing soil infiltration capacity. Compared with bare soil land and erect grass, *E. ophiurooides* (stolon grass) was observed to perform best in delaying the time of surface flow generation. By contrast, *L. perenne* (erect grass) had a tufted morphology and sparse roots resulting in relatively less soil porosity.

4.2. Effects of grass species on hydraulic and hydrodynamic characteristics

Excepted for the role of grass in altering rainfall redistribution, stolon and erect grass species exerted different effects on flow pathway (Dong et al., 2018; Wang et al., 2021b), which led to the differences of water flow movement and hydraulic and hydrodynamic characteristics (Wei et al., 2014; Nicosia et al., 2020). The maximum v occurred on the BSP, while *E. ophiurooides* and *L. perenne* effectively decreased mean v by 64.1 % and 38.4 %, respectively. The mean v for the *E. ophiurooides* plots (2.7×10^{-2} m/s) was significantly lower than that for the *L. perenne* plots (4.7×10^{-2} m/s), which is confirmed by Zhang et al (2020), who explained that the difference in v variation between two grass species (*Melinis minutiflora* and *Chrysopogon zizanioides*) was mainly due to their grass components. The creeping interlaced roots of the *E. ophiurooides* grass had the more capability in intercepting and slowing down the surface flow, even under a low coverage. Though the *L. perenne* had dense roots and stems above-ground, the erect root systems still provided numerous gaps to allow surface flow to path through, moreover, the creeping interlaced roots provided a higher surface roughness nearby the ground than the erect roots system (Pan et al., 2019; Li et al., 2021; Duan et al., 2022). The hydraulic parameters like f , Fr and n also proved the differences. The f for the grass-covered plots was higher than that for the BSP, with mean values of 397.74 (*E. ophiurooides* plots) and 91.26 (*L. perenne* plots) higher than BSP (21.49), respectively. The mean Fr -values for the BSP were clearly more than one, while for the grass-covered plots were below one. Some observations have demonstrated the impacts and differences of grass species above- and below-ground parts in altering the surface flow hydraulic and hydrodynamic parameters (Pan et al., 2016; Li et al., 2021). Li et al. (2021) also revealed that grass stems, leaves and roots played important roles in increasing the critical hydrodynamic forces and resistance coefficient thus reducing flow velocity and stream power. Specifically, the grass stems and leaves change the diameter of the raindrops by intercepting and buffering them, hence attenuating their kinetic energy (Zhao et al., 2017; Zhang et al., 2020; Wang et al., 2021b). The denser root systems of *E. ophiurooides* could significantly promote the soil agglomerate formation and enhance soil erosion resistance through the interpenetration and entanglement of soil particles (Xiao et al., 2011; Li et al., 2021; Jafarpoor et al., 2022). The root diameter of *E. ophiurooides* was coarser and thicker than *L. perenne* which decreased the soil erodibility better, because fine roots could attain the quicker root growth and decay than coarse roots (Fattet et al., 2011; Wang et al., 2018; Wang et al., 2021a). Additionally, the *E. ophiurooides* was composed of large amount of dense fibrous roots, which could cause “wrapping and twisting” of the surrounding soil mass in a three-dimensional stress state; hence, the soil

shear strength was enhanced (Li et al., 2021; Wang et al., 2021a, b).

4.3. Effects of grass species on soil loss

A comprehensive understanding of the impact of runoff processes, hydraulic and hydrodynamic characteristics on sediment yield would greatly facilitate future soil erosion control (Duan et al., 2022). Specifically, raindrops fall from a high altitude with speed and energy, transforming the potential energy of water droplets into kinetic energy, which damage soil structure, disperse the soil aggregates and produce more transportable sediment (Jiang et al., 2018; Li et al., 2021). The largest mean sediment concentration, soil loss, and D_{50} values were found on bare soil land (Table 4, Fig. 6). The conclusion was consistent with the results of Zhou and Shangguan (2007), who reported the greater capability of *L. perenne* in reducing soil loss compared with bare soil. Explanations were found in Fattet et al. (2011) and Hatefi et al. (2020), who proposed that grass roots could contributed to suppressing the movement of sediments by releasing root exudates, which increased the soil particle viscosity and soil aggregate stability. Furthermore, ten grasslands were investigated by Wang et al. (2018), who demonstrated that grass species and their root systems could significantly change the process of soil detachment and result in great differences in sediment yield. In general, grass improved soil physical properties and enhanced their anti-scouring ability through the interpenetration and winding of soil particles, thus reducing sediment concentrations and soil loss (Guo et al., 2020; Zhang et al., 2022).

The results revealed that the sediment yield decreased with the increment of grass density (Li et al., 2009; Zhang et al., 2022). As the grass coverage increased from 30 % to 70 %, the sediment concentration decreased by 44.5 % and 60.0 % on *E. ophiurooides* and *L. perenne* plots, respectively. Moreover, the results showed D_{50} decreased with increasing coverage, consistent with the variation trends of surface flow and velocity with grass density. When grass coverage increased from 30 % to 70 %, the *E. ophiurooides* and *L. perenne* plots presented a decreasing average D_{50} varying from 36.3 to 28.5 μm and 61.4 to 55.7 μm , respectively (Fig. 7). Many previous experiments from different regions also highlighted that the increased grass cover further weakened the impact of raindrop splash erosion, reduced the transportation capacity of overland flow, and trapped sediment (Li et al., 2009; Sun et al., 2019; Jafarpoor et al., 2022).

Distinct response of sediment yield and soil erosion processes appeared among stolon and erect grass species (Li and Pan, 2018). Statistics indicated that D_{50} for stolon grass was smaller than that of erect grass. The lowest D_{50} occurred for the *E. ophiurooides* plots, with total average values of 32.4 μm . Moreover, the mean D_{50} and soil loss rate for the *L. perenne* plots were 1.8 and 3.1 times higher than that for the *E. ophiurooides* plots, respectively. These results suggested that the stolon grass performed better in depressing flow scouring and shearing on the surface and improving the efficiency of soil erosion reduction. An explanation reported by Zheng et al. (2008) and Duan et al. (2016) was that grass canopies and roots were critical factors that determined the magnitude of soil loss. *E. ophiurooides* had relatively higher root density and larger root diameter, and these root traits were experimentally confirmed to reduce soil detachment and transportation by Wang et al. (2018) and Wang et al. (2021a). According to some studies, grass components affected the composition and structure of soil particles as well as the vertical movement channel and flow section of soil water, thus changing the water and sediment movement and forming rill erosion (Cao et al., 2015; Wang et al., 2021b). As shown in Fig. 8, the rill erosion dominated the bare land plots, especially under larger rainfall intensity, and the concentrated water flowed faster along the multiple rills, which was also observed by previous research (Gyssels and Poesen, 2003; Palmeri et al., 2018). Pan et al. (2019) suggested that the grass measures could control the development and occurrence of rill erosion. There was no obvious rills development on the *E. ophiurooides* plots in our experiments. However, the erect grass of *L. perenne* made the surface

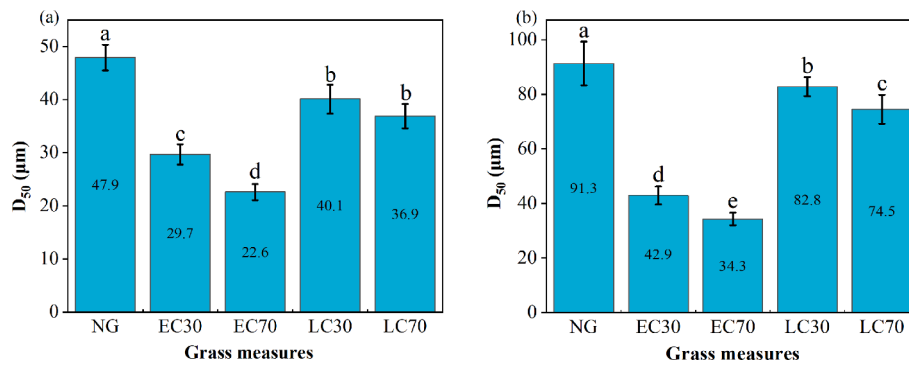


Fig. 6. The average value of D_{50} under different grass measures: (a) rainfall intensity 60 mm h^{-1} , (b) rainfall intensity 120 mm h^{-1} . Values with superscript letters (a–e) are significantly different across columns at the $\alpha = 0.05$ level using LSD analyses.

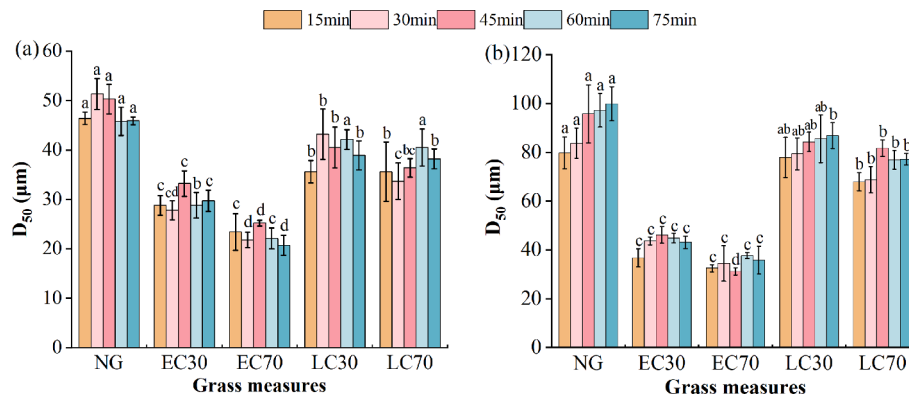


Fig. 7. Variation of D_{50} under different grass measures over time: (a) rainfall intensity 60 mm h^{-1} , (b) rainfall intensity 120 mm h^{-1} .

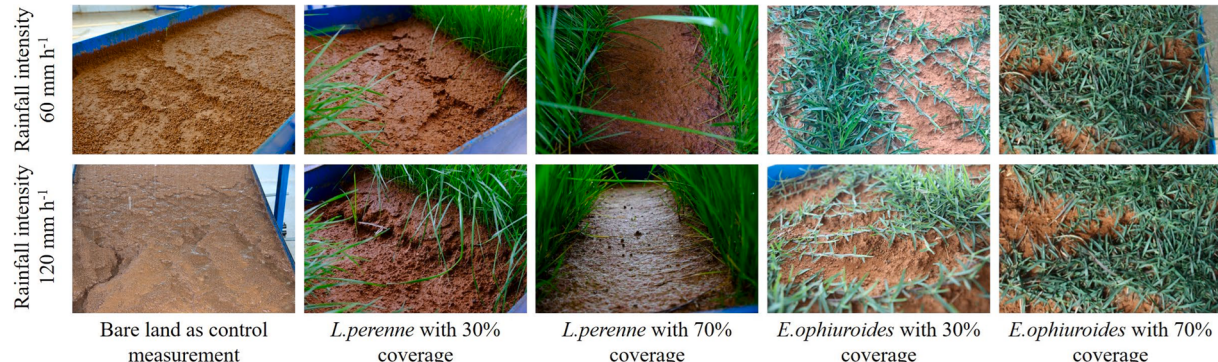


Fig. 8. The view of two grass components in soil erosion resistance.

flow channel relatively narrow and curved, resulting in the development of rills, which increased sediment yield and soil loss several times (Zhang et al., 2018; Wang et al., 2021a; Jafarpoor et al., 2022).

The roles of grass and their components decreased with increasing rainfall intensities (Zhang et al., 2020; Li et al., 2021). The study found that the mean D_{50} under RI₆₀ (35.4 μm) was significantly lower than that under RI₁₂₀ (65.2 μm). This was related to stronger raindrop splash and runoff scouring influenced by increasing precipitation. Arnaez et al. (2007) elucidated that grass was more conducive to erosion caused by low rainfall intensity. Specifically, the heavy precipitation events accelerate soil erosion causing the disruption of soil aggregates and produce more transportable sediment, and the ability of grass to trap sediment would be weakened (Nespoulous et al., 2019; Zhang et al., 2020). Therefore, the integration of grass planting and other supplemental measures should be implemented scientifically in some extreme

rainfall events (Kheirfam et al., 2020). Noteworthy, even under heavy rainfall with intensity of 120 mm h^{-1} , the sediment conservation efficiency of $E.\text{ophiuroides}$ reached 88.0 % at low cover and 94.0 % at high cover, with values of 30.0 % and 10.0 % higher than $L.\text{perenne}$, respectively. Thus, the stolon grass showed a considerable improvement in sediment and flow trapping efficacy, which was more important to control the concentrated flow scouring under extreme rainfall events.

5. Conclusions

This study focused on exploring two grass species on surface-subsurface flow generation, sediment loss, and hydraulic and hydrodynamic characteristics in the red soil hilly region. The surface flow and sediment generation on bare land were significantly higher compared to grass-covered land, indicating that grass species played

important roles in controlling soil loss. The *E. ophiuroides* plots generally showed the lower surface flow and higher subsurface flow than the *L. perenne* plots. The lower *Fr* and higher *f* occurred on *E. ophiuroides* compared to other treatments. All the experimental plots exhibited laminar flow (*Re* < 100). The mean velocity was in the decreasing order of bare plot > *L. perenne* > *E. ophiuroides*. These results highlighted that *E. ophiuroides* performed better than *L. perenne* in soil and water conservation.

The different roles of the two grass species in controlling soil erosion are mainly due to their above-ground (canopy density, leaf area, quality and hardness, stem, etc.) and under-ground parts (root systems, etc.). Grass coverage and rainfall intensity were important determinants of soil erosion. Stolon grass represented by *E. ophiuroides* performed the best in controlling soil loss than erect grass represented by *L. perenne*, even in low coverage and high rainfall intensity. The practical benefits of stolon grass were more available and easier to achieve in the fields. Therefore, stolon grass (such as *E. ophiuroides*) is highly recommended for soil and water conservation when concerned with concentration flow scouring and extreme rainfall events in the changing climate conditions.

CRediT authorship contribution statement

Zhimin Yang: Data curation, Formal analysis, Investigation, Methodology, Writing – original draft, Writing – review & editing. **Chunhui Li:** Methodology, Supervision, Validation, Writing – review & editing. **Yaojun Liu:** Funding acquisition, Resources, Supervision, Validation, Writing – review & editing. **Jian Duan:** Investigation, Resources, Visualization. **Lichao Zhang:** Formal analysis, Supervision. **Zhongwu Li:** Validation, Writing – review & editing. **Xianguo Zhou:** Data curation. **Qi Li:** Data curation. **Yichun Ma:** Investigation. **Liang Tian:** Formal analysis.

Declaration of Competing Interest

The authors declare that they have no known competing financial interests or personal relationships that could have appeared to influence the work reported in this paper.

Data availability

Data will be made available on request.

Acknowledgements

This work was supported by the National Natural Science Foundation of China (41877084; 41967012; 42107378; 41501287), Hunan Normal University Student Innovation Project (S202110542121; 2022057). We would like to extend special thanks to the editor and reviewers for insightful advice and comments on the manuscript.

References

- Arnaez, J., Lasanta, T., Ruiz-Flaño, P., Ortigosa, L., 2007. Factors affecting runoff and erosion under simulated rainfall in Mediterranean vineyards. *Soil Tillage Res.* 93 (2), 324–334. <https://doi.org/10.1016/j.still.2006.05.013>.
- Cao, L., Liang, Y., Wang, Y., Lu, H., 2015. Runoff and soil loss from *Pinus massoniana* forest in southern China after simulated rainfall. *Catena* 129, 1–8. <https://doi.org/10.1016/j.catena.2015.02.009>.
- De Baets, S., Poessens, J., Knapen, A., Barberá, G.G., Navarro, J.A., 2007. Root characteristics of representative Mediterranean plant species and their erosion-reducing potential during concentrated runoff. *Plant Soil.* 294 (1), 169–183. <https://doi.org/10.1007/s11104-007-9244-2>.
- Digiovanni-White, K., Montalto, F., Gaffin, S., 2018. A comparative analysis of micrometeorological determinants of evapotranspiration rates within a heterogeneous urban environment. *J. Hydrol.* 562, 223–243. <https://doi.org/10.1016/j.jhydrol.2018.04.067>.
- Dong, Y., Xiong, D., Su, Z.A., Yang, D., Zheng, X., Shi, L., Poessens, J., 2018. Effects of vegetation buffer strips on concentrated flow hydraulics and gully bed erosion based on in situ scouring experiments. *Land Degrad Dev.* 29 (6), 1672–1682. <https://doi.org/10.1002/ldr.2943>.
- Duan, L.X., Huang, M.B., Zhang, L.D., 2016. Differences in hydrological responses for different vegetation types on a steep slope on the Loess Plateau, China. *J. Hydrol.* 537, 356–366. <https://doi.org/10.1016/j.jhydrol.2016.03.057>.
- Duan, J., Liu, Y.J., Wang, L.Y., Yang, J., Tang, C.J., Zheng, H.J., 2022. Importance of grass stolons in mitigating runoff and sediment yield under simulated rainstorms. *Catena* 213, 106132. <https://doi.org/10.1016/j.catena.2022.106132>.
- El Kateb, H., Zhang, H., Zhang, P., Mosandl, R., 2013. Soil erosion and surface runoff on different vegetation covers and slope gradients: a field experiment in Southern Shaanxi Province, China. *Catena* 105, 1–10.
- Fattet, M., Fu, Y., Ghoshem, M., Ma, W., Foulonneau, M., Nespolous, J., Bissonnais, Y.L., Stokes, A., 2011. Effects of vegetation type on soil resistance to erosion: relationship between aggregate stability and shear strength. *Catena* 87, 60–69. <https://doi.org/10.1016/j.catena.2011.05.006>.
- Gao, L., Bowker, M.A., Xu, M., Sun, H., Tu, D., Zhao, Y., 2017. Biological soil crusts decrease erodibility by modifying inherent soil properties on the Loess Plateau, China. *Soil Biol. Biochem.* 105, 49–58. <https://doi.org/10.1016/j.soilbio.2016.11.009>.
- Gómez, J.A., Nearing, M.A., 2005. Runoff and sediment losses from rough and smooth soil surfaces in a laboratory experiment. *Catena* 59 (3), 253–266. <https://doi.org/10.1016/j.catena.2004.09.008>.
- Guo, M.M., Wang, W.L., Wang, T.C., Wang, W.X., Kang, H.L., 2020. Impacts of different vegetation restoration options on gully head soil resistance and soil erosion in loess tablelands. *Earth Surf Process Landf.* 45 (4), 1038–1050. <https://doi.org/10.1002/esp.4798>.
- Gyssels, G., Poessens, J., 2003. The importance of plant root characteristics in controlling concentrated flow erosion rates. *Earth Surf Process Landf.* 28, 371–384. <https://doi.org/10.1002/esp.447>.
- Hatefi, M., Sadeghi, S.H., Erfanzadeh, R., Behzadfar, M., 2020. Inhibiting soil loss and runoff from small plots induced by an individual freeze-thaw cycle using three rangeland species. *Int. Soil Water Conserv. Res.* 8 (3), 228–236. <https://doi.org/10.1016/j.jiswcr.2020.05.004>.
- Issas, 1978. *Soil Physical and Chemical Analysis*. Shanghai Science and Technology Press, Shanghai (in Chinese).
- Jafarpoor, A., Sadeghi, S.H., Darki, B.Z., Homaei, M., 2022. Changes in morphologic, hydraulic, and hydrodynamic properties of rill erosion due to surface inoculation of endemic soil cyanobacteria. *Catena* 208, 105782. <https://doi.org/10.1016/j.catena.2021.105782>.
- Jiang, F., Zhan, Z., Chen, J., Lin, J., Wang, M.K., Ge, H., Huang, Y., 2018. Rill erosion processes on a steep colluvial deposit slope under heavy rainfall in flume experiments with artificial rain. *Catena* 169, 46–58. <https://doi.org/10.1016/j.catena.2018.05.023>.
- Kheirfam, H., Sadeghi, S.H., Darki, B.Z., 2020. Soil conservation in an abandoned agricultural rain-fed land through inoculation of cyanobacteria. *Catena* 187, 104341. <https://doi.org/10.1016/j.catena.2019.104341>.
- Li, J.M., Li, L., Wang, Z.G., Zhang, C.W., Wang, Y.F., Wang, W.L., Zhang, G.H., Huang, J.Q., Li, H., Lv, X.D., Pu, J., Liu, J.G., 2021. The contributions of the roots, stems, and leaves of three grass species to water erosion reduction on spoil heaps. *J. Hydrol.* 603 (PB), 127003 <https://doi.org/10.1016/j.jhydrol.2021.127003>.
- Li, C.J., Pan, C.Z., 2018. The relative importance of different grass components in controlling runoff and erosion on a hillslope under simulated rainfall. *J. Hydrol.* 558, 90–103. <https://doi.org/10.1016/j.jhydrol.2018.01.007>.
- Li, M., Yao, W., Ding, W., Yang, J., Chen, J., 2009. Effect of grass coverage on sediment yield in the hillslope-gully side erosion system. *J. Geogr. Sci.* 19 (3), 321–330. <https://doi.org/10.1007/s11442-009-0321-8>.
- Li, Z., Zhang, G., Geng, R., Wang, H., Zhang, X., 2015. Land use impacts on soil detachment capacity by overland flow in the Loess Plateau, China. *Catena* 124, 9–17. <https://doi.org/10.1016/j.catena.2014.08.019>.
- Liu, Y.J., Yang, J., Hu, M., Tang, C.J., Zhen, H.J., 2016a. Characteristics of the surface-subsurface flow generation and sediment yield to the rainfall regime and land-cover by long-term in-situ observation in the red soil region, South China. *J. Hydrol.* 539, 457–467. <https://doi.org/10.1016/j.jhydrol.2016.05.058>.
- Liu, Y.J., Hu, J.M., Wang, T.W., Cai, C.F., Li, Z.X., Zhang, Y., 2016b. Effects of vegetation cover and road-concentrated flow on hillslope erosion in rainfall and scouring simulation tests in the Three Gorges Reservoir Area, China. *Catena* 136, 108–117. <https://doi.org/10.1016/j.catena.2015.06.006>.
- Ma, Y., Li, Z., Deng, C., Yang, J., Tang, C., Duan, J., Zhang, Z.W., Liu, Y., 2022. Effects of tillage-induced soil surface roughness on the generation of surface-subsurface flow and soil loss in the red soil sloping farmland of southern China. *Catena* 213, 106230. <https://doi.org/10.1016/j.catena.2022.106230>.
- Nespoulous, J., Merino-Martín, L., Monnier, Y., Bouchet, D.C., Ramel, M., Dombeuf, R., Viennois, G., Mao, Z., Zhang, Z.L., Cao, K.B., Bissonnais, Y.L., Sidle, R.C., Stokes, A., 2019. Tropical forest structure and understorey determine subsurface flow through biopores formed by plant roots. *Catena* 181, 104061. <https://doi.org/10.1016/j.catena.2019.05.007>.
- Nicosia, A., Di Stefano, C., Pampalone, V., Palmeri, V., Ferro, V., Polyakov, V., Nearing, M.A., 2020. Testing a theoretical resistance law for overland flow under simulated rainfall with different types of vegetation. *Catena* 189, 104482. <https://doi.org/10.1016/j.catena.2020.104482>.
- Palmeri, V., Pampalone, V., Di Stefano, C., Nicosia, A., Ferro, V., 2018. Experiments for testing soil texture effects on flow resistance in mobile bed rills. *Catena* 171, 176–184. <https://doi.org/10.1016/j.catena.2018.07.016>.
- Pan, C.Z., Shangguan, Z.P., Lei, T.W., 2006. Influences of grass and moss on runoff and sediment yield on sloped loess surfaces under simulated rainfall. *Hydrolog. Process.* 20 (18), 3815–3824. <https://doi.org/10.1002/hyp.6158>.

- Pan, C.Z., Ma, L., Wainwright, J., 2016. Particle selectivity of sediment deposited over grass barriers and the effect of rainfall. *Water Resour. Res.* 52 (10), 7963–7979. <https://doi.org/10.1002/2016WR019010>.
- Pan, C.Z., Shangguan, Z.P., 2006. Runoff hydraulic characteristics and sediment generation in sloped grassplots under simulated rainfall conditions. *J. Hydrol.* 331 (1–2), 178–185. <https://doi.org/10.1016/j.jhydrol.2006.05.011>.
- Pan, D., Yang, S., Song, Y., Gao, X., Wu, P., Zhao, X., 2019. The tradeoff between soil erosion protection and water consumption in revegetation: Evaluation of new indicators and influencing factors. *Geoderma* 347, 32–39. <https://doi.org/10.1016/j.geoderma.2019.02.003>.
- Sadeghi, S.H.R., Sharifi Moghadam, E., Khaledi Darvishan, A., 2016. Effects of subsequent rainfall events on runoff and soil erosion components from small plots treated by vinasse. *Catena* 138, 1–12. <https://doi.org/10.1016/j.catena.2015.11.007>.
- Sadeghi, S.H., Singh, V.P., Kiani-Harchegani, M., Asadi, H., 2018. Analysis of sediment rating loops and particle size distributions to characterize sediment source at mid-sized plot scale. *Catena* 167, 221–227. <https://doi.org/10.1016/j.catena.2018.05.002>.
- Sadeghi, S.H., Ghaffari, G.A., Rangavar, A., Hazbavi, Z., Singh, V.P., 2020. Spatiotemporal distribution of soil moisture in gully facies. *Int. Soil Water Conserv. Res.* 8 (1), 15–25. <https://doi.org/10.1016/j.iswcr.2019.10.001>.
- Sadeghi, S.M.M., Van Stan, J.T., Pykner, T.G., Friesen, J., 2017. Canopy hydrometeorological dynamics across a chronosequence of a globally invasive species, *Ailanthus altissima* (Mill., tree of heaven). *Agric. For. Meteorol.* 240–241, 10–17.
- Shi, Z.H., Yue, B.J., Wang, L., Fang, N.F., Wang, D., Wu, F.Z., 2013. Effects of mulch cover rate on interrill erosion processes and the size selectivity of eroded sediment on steep slopes. *Soil Sci. Soc. Am. J.* 77, 257–267. <https://doi.org/10.2136/sssaj2012.0273>.
- Sun, W., Mu, X., Gao, P., Zhao, G., Li, J., Zhang, Y., Chiew, F., 2019. Landscape patches influencing hillslope erosion processes and flow hydrodynamics. *Geoderma* 353, 391–400. <https://doi.org/10.1016/j.geoderma.2019.07.003>.
- Tong, X.W., Brandt, M., Yue, Y.M., Horion, S., Wang, K., Keersmaecker, W.D., Tian, F., Schurgers, C., Xiao, X.M., Luo, Y.Q., Chen, C., Myneni, R., Shi, Z., Chen, H.S., Fensholt, R., 2018. Increased vegetation growth and carbon stock in China karst via ecological engineering. *Nat. Sustain.* 1 (1), 44–50. <https://www.nature.com/article/s41893-017-0004-x>.
- Tu, A., Xie, S., Zheng, H., Li, H., Li, Y., Mo, M., 2021. Long-term effects of living grass mulching on soil and water conservation and fruit yield of citrus orchard in south China. *Agric. Water Manag.* 252, 106897. <https://doi.org/10.1016/j.agwat.2021.106897>.
- Waldron, L.J., Dakessian, S., 1981. Soil reinforcement by roots: calculation of increased soil shear resistance from root properties. *Soil Sci.* 132 (6), 427–435. <https://doi.org/10.1097/00010694-198112000-00007>.
- Wang, B., Zhang, G.H., Yang, Y.F., Li, P.P., Liu, J.X., 2018. The effects of varied soil properties induced by natural grassland succession on the process of soil detachment. *Catena* 166, 192–199. <https://doi.org/10.1016/j.catena.2018.04.007>.
- Wang, B., Li, P.P., Huang, C.H., Liu, G.B., Yang, Y.F., 2021a. Effects of root morphological traits on soil detachment for ten herbaceous species in the Loess Plateau. *Sci. Total Environ.* 754, 142304. <https://doi.org/10.1016/j.scitotenv.2020.142304>.
- Wang, L., Zhang, G., Zhu, P., Wang, X., 2020. Comparison of the effects of litter covering and incorporation on infiltration and soil erosion under simulated rainfall. *Hydro. Process.* 34 (13), 2911–2922. <https://doi.org/10.1002/hyp.13779>.
- Wang, L., Zhang, Y., Jia, J., Chen, Q., Zhang, X., 2021b. Effect of vegetation on the flow pathways of steep hillslopes. Overland flow plot-scale experiments and their implications. *Catena* 204, 105438. <https://doi.org/10.1016/j.catena.2021.105438>.
- Wei, W., Jia, F., Yang, L., Chen, L., Zhang, H., Yu, Y., 2014. Effects of surficial condition and rainfall intensity on runoff in a loess hilly area, China. *J. Hydrol.* 513, 115–126. <https://doi.org/10.1016/j.jhydrol.2014.03.022>.
- Wuepper, D., Borrelli, P., Finger, R., 2019. Countries and the global rate of soil erosion. *Nat. Sustain.* 3 (1), 51–55. <https://doi.org/10.1038/s41893-019-0438-4>.
- Xiao, B., Wang, Q.H., Wang, H.F., Dai, Q.H., Wu, J.Y., 2011. The effects of narrow grass hedges on soil and water loss on sloping lands with alfalfa (*Medicago sativa* L.) in Northern China. *Geoderma* 167, 91–102. <https://doi.org/10.1016/j.geoderma.2011.09.010>.
- Zhang, X., Li, P., Li, Z.B., Yu, G.Q., Li, C., 2018. Effects of precipitation and different distributions of grass strips on runoff and sediment in the loess convex hillslope. *Catena* 162, 130–140. <https://doi.org/10.1016/j.catena.2017.12.002>.
- Zhang, S.Y., Li, C., Huang, B., Liu, T., Guo, T.L., Yuan, Z.J., He, B., Li, D.Q., 2020. Flow hydraulic responses to near-soil surface components on vegetated steep red soil colluvial deposits. *J. Hydrol.* 582, 124527. <https://doi.org/10.1016/j.jhydrol.2019.124527>.
- Zhang, X., Song, J., Wang, Y., Sun, H., Li, Q., 2022. Threshold effects of vegetation coverage on runoff and soil loss in the Loess Plateau of China: a meta-analysis. *Geoderma* 412, 115720. <https://doi.org/10.1016/j.geoderma.2022.115720>.
- Zhao, C.H., Gao, J.E., Huang, Y.F., Wang, G.Q., Xu, Z., 2017. The contribution of *Astragalus adsurgens* roots and canopy to water erosion control in the water-wind crisscrossed erosion region of the Loess Plateau, China. *Land Degrad. Dev.* 28 (1), 265–273. <https://doi.org/10.1002/ldr.2508>.
- Zheng, H., Chen, F.L., Ouyang, Z.Y., Tu, N.M., Xu, W.H., Wang, X.K., Miao, H., Li, X.Q., Tian, Y.X., 2008. Impacts of reforestation approaches on runoff control in the hilly red soil region of southern China. *J. Hydrol.* 356, 174–184. <https://doi.org/10.1016/j.jhydrol.2008.04.007>.
- Zheng, H.J., Hu, J.M., Huang, P.F., Wang, L.Y., Wan, J.L., 2014. Comparative study of nitrogen and phosphorus through surface-flow and interflow on red soil farmland. *J. Soil Water Conserv.* 28 (6), 41–45 + 70 (In Chinese).
- Zhou, Z.C., Shangguan, Z.P., 2007. The effects of ryegrass roots and shoots on loess erosion under simulated rainfall. *Catena* 70 (3), 350–355. <https://doi.org/10.1016/j.catena.2006.11.002>.